Emission spectra of HeAr2+ and HeKr2+ heterotrimer ions produced in a helium flowing afterglow

ARTICLE *in* CHEMICAL PHYSICS · SEPTEMBER 1998

Impact Factor: 1.65 · DOI: 10.1016/S0301-0104(98)00182-7

5 AUTHORS, INCLUDING:

Masaharu Tsuji

Kyushu University

441 PUBLICATIONS **6,229** CITATIONS

ELSEVIER

Chemical Physics 236 (1998) 319–329

Chemical Physics

Emission spectra of $HeAr_2^+$ and $HeKr_2^+$ heterotrimer ions produced in a helium flowing afterglow

Masaharu Tsuji [a,b,*], Makoto Tanaka [b,1], Erika Oda [b], Hiroaki Ishimi [b,2], Yukio Nishimura [a,b]

[a] *Institute of Advanced Material Study, Kyushu University, Kasuga-shi, Fukuoka 816-8580, Japan*

[b] *Department of Molecular Science and Technology, Graduate School of Engineering Sciences, Kyushu University, Kasuga-shi, Fukuoka 816-8580, Japan*

Received 21 April 1998

Abstract

Emission spectra resulting from clustering reactions of He^+ with a heavier rare gas Rg(Rg = Ne, Ar, or Kr) have been studied in a helium flowing afterglow at various stagnation pressures of Rg. At low stagnation pressures, emission spectra of $HeRg^+$ heterodimer ions were found for Rg = Ne, Ar, and Kr due to radiative association and three-body clustering reactions. At high stagnation pressures, new continuous bands were found for Rg = Ar and Kr at longer-wavelength region of the heterodimer bands. They were attributed to bound-free transitions of $HeRg_2^+$ heterotrimer ions. The $HeRg_2^+$ bands consisted of two components: the first continuum degraded to the red from near the $HeRg^+(B^2\Sigma^+–X^2\Sigma^+)$ transition, and the second continuum, a roughly Gaussian feature at longer wavelengths. The first and second components were ascribed to the $B\,1/2–X\,1/2$ and $B\,1/2–A_2\,1/2$ transitions of $HeRg_2^+$, respectively. The emission intensity of the second continuum increased more rapidly than that of the first one with increasing the stagnation pressure of Rg or a foreign gas. It was explained by the fact that the second continuum arises dominantly from low vibrationally excited levels formed by collisional relaxation of the upper vibrational levels of $HeRg_2^+(B\,1/2)$. The geometries of $HeRg_2^+$ in the upper $B\,1/2$ state and the lower $X\,1/2$ and $A_2\,1/2$ states were attributed to $Rg\cdots He^+Rg$ and $Rg\cdots HeRg^+$, respectively, and the bound-free character derives from attractive $Rg\cdots He^+$ and repulsive $Rg\cdots He$ bonds in $Rg\cdots(HeRg)^+$.

1. Introduction

Tanaka et al. [1] have found that an electronic discharge in a binary mixture of rare gases provides several discrete emission band groups confined to a narrow wavelength region characteristic of the pair of rare gases and closely related in energy to the ionization energy difference between the two atoms. Such spectra were observed for nine of the ten binary mixtures of He, Ne, Ar, Kr, and Xe. These bands were ascribed to a bound–bound charge-transfer transition $Rg^+Rg' \rightarrow RgRg'^+$, in which Rg is the lighter and Rg′ the heavier element in the mixture. The validity of their assignment was confirmed by later high-resolution rotational analyses of $HeAr^+$, $HeNe^+$, and $ArKr^+$ [2–4].

* Corresponding author.

[1] Present address: Nippon Sanso, Tsukuba, Ibaragi, Japan.

[2] Present address: the Labor Standard Inspection Office, Osaka, Japan.

0301-0104/98/$ - see front matter
PII: S0301-0104(98)00182-7

As an example of the energy diagram of $HeRg^+$, an energy diagram of $HeAr^+$ is shown in Fig. 1. There are single upper state ($B\,^2\Sigma^+$) derived from the $He^+(^2S_{1/2}) + Ar(^1S_0)$ dissociation limit and three lower states ($X\,^2\Sigma^+$, $A_1\,^2\Pi_{3/2}$, $A_2\,^2\Pi_{1/2}$) correlating with the $He(^1S_0) + Ar^+(^2P_{3/2,1/2})$ dissociation limits. In general, only the two parallel transitions ($\Delta\Omega = 0$), denoted by A and D, have appreciable intensities among the three dipole-allowed transitions ($\Delta\Omega = 0, \pm 1$) [2,3]. The dissociation energy (D_0') of $HeRg^+(B\,^2\Sigma^+)$ has been determined to be 292.8, 1256, and 1800 cm^{-1}, for Rg = Ne, Ar, and Kr, respectively [2–4].

Although extensive spectroscopic studies had been carried out on electronic structures and formation mechanisms of rare gas heterodimer ions such as $HeAr^+$ and $HeNe^+$ [1–13], no optical study had been made for further larger heterocluster ions until our recent studies [14–16]. We have recently investigated emission spectra resulting from clustering reactions of a rare gas ion Rg^+(Rg = Ne, Ar, Kr) with a heavier rare gas Rg′(Rg′ = Ar, Kr, Xe) in rare gas flowing afterglows at various stagnation pressures of Rg′. At low stagnation pressures of Rg′, emission spectra of $NeRg'^+$(Rg′ = Ar, Kr, Xe), $ArRg'^+$(Rg′ = Kr, Xe), and $KrXe^+$ heterodimer ions were found due to radiative association and three-body clustering reactions. At high stagnation pressures of Rg′, new continuous bands were found at longer-wavelength region of the heterodimer bands in most cases. They were attributed to bound-free transitions of $NeRg_2'^+$(Rg′ = Ar, Kr, Xe), $ArRg_2'^+$(Rg′ = Kr, Xe), and $KrXe_2^+$ heterotrimer ions. In most cases, the $RgRg_2'^+$ bands consisted of two components: the first continuum degraded to the red from near the

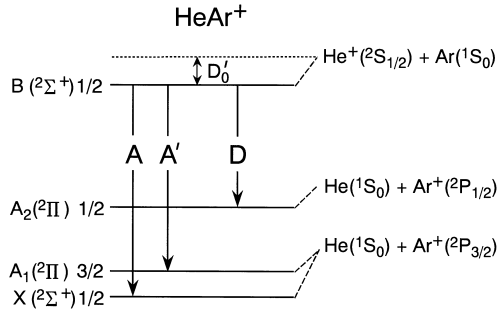

Fig. 1. Energy-level diagram of the $HeAr^+$ cluster ion.

$B\,1/2–X\,1/2$ and $C_1\,3/2–A_1\,3/2$ transitions of the $RgRg'^+$ bands, and the second continuum, a roughly Gaussian feature at longer wavelengths. It was found that the lower $Rg^+(^2P_{3/2})$ components were responsible for the formation of $RgRg_2'^{+*}$ by isolating one of the spin–orbit states of Rg^+, $^2P_{1/2}$ or $^2P_{3/2}$. The first and second components were ascribed to the $B\,1/2–X\,1/2$ and/or $C_1\,3/2–A_1\,3/2$ transitions and the $B\,1/2–A_2\,1/2$ transition of $RgRg_2'^+$, respectively. The emission intensity of the second continuum increased more rapidly than that of the first one with increasing the stagnation pressure of Rg′ or a foreign gas. It was explained as due to the fact that the first continuum arises from high vibrational levels near the dissociation limits, while the second one occurs dominantly from low vibrational levels formed by collisional relaxation of the upper vibrational levels.

In the present study, clustering reactions leading to $HeRg_n^+$(Rg = Ne, Ar, Kr) ions have been studied in a He flowing afterglow. New broad bands, which can be ascribed to $HeRg_2^+$ bands, are observed except for the case of Rg = Ne. Their electronic transitions and formation mechanism are discussed. Preliminary results for the $HeAr_n^+$ bands resulting from the He afterglow reactions of Ar have been communicated [14]. Further experimental data obtained here suggested that our previous assignment for the $HeAr_n^+$ bands should be revised.

2. Experimental

The He flowing-afterglow apparatus used in this study was essentially identical to that reported previously [16,17]. For the generation of $HeRg_n^{+*}$(Rg = Ne, Ar, Kr), active species of helium [$He(2^3S)$, He^+, and He_2^+] were generated by a microwave discharge of high-purity helium gas operated at ~0.8–1.4 Torr (1 Torr = 133.3 Pa) with constant mass flow rates of 6000–10000 sccm ($cm^3\ min^{-1}$ at the standard condition). The contribution of ionic active species to the observed emissions was examined by using a pair of ion-collector grids placed between the discharge section and the reaction zone. The sample Rg gas was injected from a stainless-steel nozzle (0.6 mm i.d.), placed parallel to the He flow, to the

discharge flow 10–20 cm downstream from the center of the discharge. The stagnation pressure was measured using a high-pressure gauge. The stagnation pressure of Rg was varied from nearly zero to 3.9 atm corresponding to mass flow rates of 0–3500 sccm. Although the partial pressure of Rg was measured to be 0.1–0.48 Torr at Rg stagnation pressures of 0.5–3.9 atm by using a capacitance manometer attached to a main flow tube, the actual pressure of Rg just in the exit opening of the nozzle was expected to be close to the stagnation pressure.

The emission spectra around the Rg gas inlet were measured in the 110–200 and 200–1050 nm regions by using McPherson 218 and Spex 1250 M monochromators, respectively. Analog signals from a photomultiplier (Hamamatsu Photonics, R1459, R376, or R316-02) were converted to digital ones using an A/D converter. The digital photon signals were stored and analyzed with a microcomputer. Although emission spectra of $HeAr_n^+$ reported in the previous communication [14] were not corrected for the relative sensitivity of the monochromator and the photomultiplier, all emission spectra presented here were corrected for the spectral response using the same method as that reported previously [16].

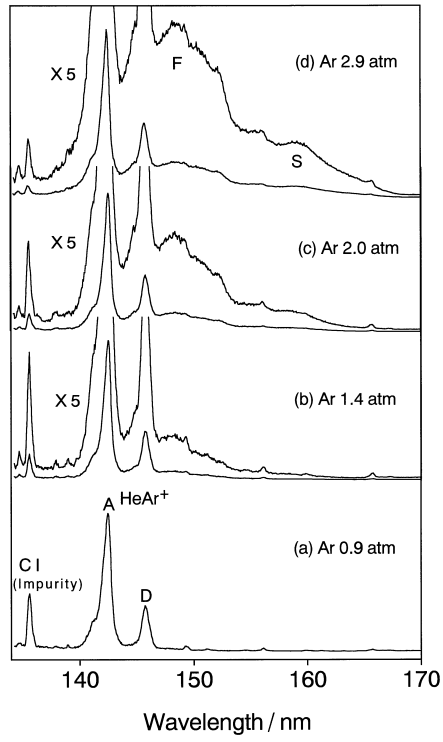

Fig. 2. Emission spectra obtained from He afterglow reactions of Ar at various Ar stagnation pressures and a constant He buffer gas pressure of 0.77 Torr. The emission intensities of each spectrum are normalized to $HeAr^+$ (A band).

3. Results and discussion

3.1. Emission spectra of $HeRg_2^+$ heterotrimer ions

Fig. 2a–d shows emission spectra obtained from the He afterglow reaction of Ar at various Ar stagnation pressures. In all the spectra, the $B^2\Sigma^+–X^2\Sigma^+$ and $B^2\Sigma^+–A_2{}^2\Pi_{1/2}$ bands of $HeAr^+$, denoted by A and D in Fig. 2a, respectively, are observed in the 140–147 nm region. Partially overlapping with these $HeAr^+$ bands, new weak broad bands appear in the red side of the heterodimer bands at high Ar stagnation pressures. The continuum consists of two components: the first one in the 137–153 nm region with a peak at $\sim$149 nm and the second one in the 153–168 nm region with a peak at $\sim$159 nm. They are denoted by F and S in Fig. 2d, respectively. The spectral features of these broad bands are very similar to those found in the Ne^+/Ar system [15,16].

Fig. 3 shows the dependence of emission intensities of $HeAr^+$(A band) and continua F and S on the Ar stagnation pressure. Continua F and S appear at higher stagnation pressures than $HeAr^+$(A band) and increase more rapidly than that with increasing the Ar stagnation pressure. This suggests that further collisions with Ar atoms or Ar_n clusters are necessary for the formation of continua F and S. Continuum S appears at a higher Ar stagnation pressure than continuum F and increases more rapidly than that at higher Ar pressures. The peak shift of the second continuum from the $HeAr^+$(B–X) band is about twice of that of the first continuum. On the basis of these two facts, we predicted that F is associated with $HeAr_2^+$ and S is related to $HeAr_3^+$ in our previous communication [14]. If this assignment is correct, little change in the S/F ratio is expected by the addition of a foreign gas such as Ne. On the other hand, an enhancement of S will occur by the addition of Ne, if the collisional relaxation participates in the formation of S. In order to examine the

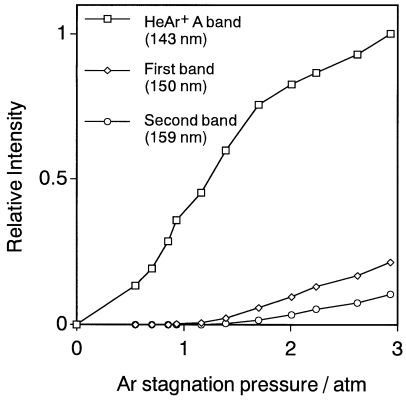

Fig. 3. The dependence of emission intensities of $HeAr^+$ (A band) and continua F and S on the Ar stagnation pressure for the He^+/Ar system.

contribution of the collisional relaxation to continuum S, Ne was premixed with Ar. Fig. 4a–d shows emission spectra obtained by adding various Ne stagnation pressures. The relative intensity of continuum S (159 nm) to that of continuum F (150 nm) increases from 0.26 to 0.36 with increasing the Ne stagnation pressure from 0 to 1.5 atm, indicating that the collisional relaxation participates in the formation of the second continuum. Although the energy shift of the peak of the second continuum from the $HeAr^+(B–X)$ band is about twice of that of the first continuum, such a relation could not be found for the two continua in the Ne^+/Rg and Ar^+/Xe systems [16]. These facts led us to conclude that our previous assignment for the second continuum is incorrect.

Fig. 5a–d shows emission spectra obtained from the He afterglow reactions of Kr at various Kr stagnation pressures. Intense A ($B^2\Sigma^+–X^2\Sigma^+$) and D ($B^2\Sigma^+–A_2{}^2\Pi_{1/2}$) bands of $HeKr^+$ and the Kr($5s\ ^3P_1 \rightarrow 4p^6\ ^1S_0$) line are found in the 117–130 nm region at a low Kr stagnation pressure of 1.0 atm. Three continuous bands appear at higher Kr stagna-

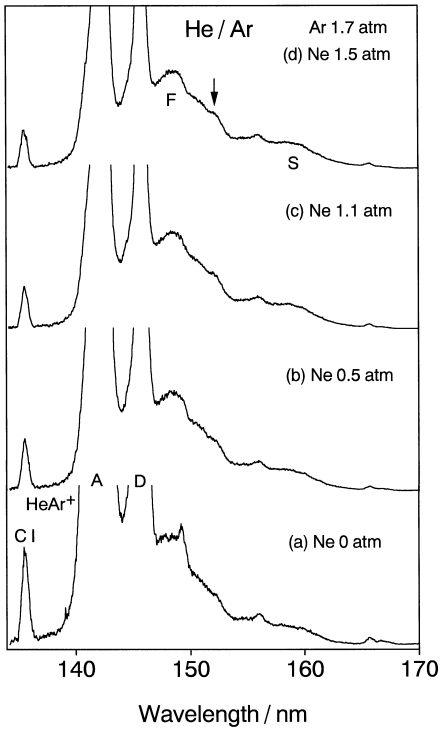

Fig. 4. Emission spectra obtained from He afterglow reactions of Ar by the addition of various stagnation pressures of Ne. The sample Ar gas was kept at a constant stagnation pressure of 1.7 atm. The emission intensities of each spectra are normalized to continuum F.

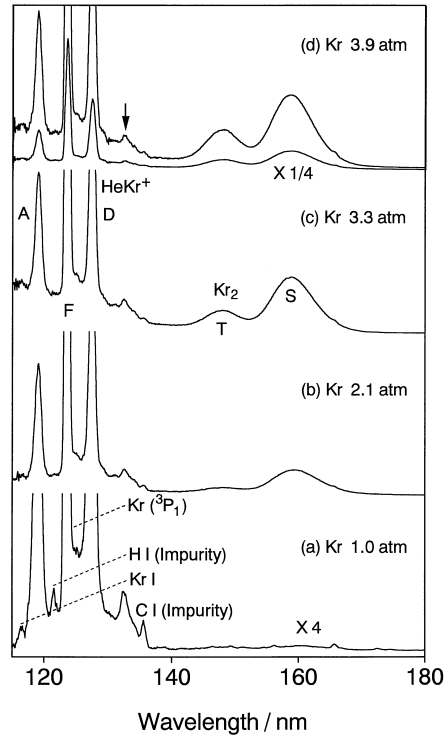

Fig. 5. Emission spectra obtained from He afterglow reactions of Kr at various Kr stagnation pressures and a constant He buffer gas pressure of 1.1 Torr. The emission intensities of each spectra are normalized to $HeKr^+$ (A band).

tion pressures. The first continuum in the 115–137 nm region (F) appears as a weak underground band of the A and D bands of $HeKr^+$, while the second and third continua with typical Gaussian type envelopes appear in the 148–170 nm region (S) and 142–152 nm region (T), respectively. The observed wavelength of the third continuum is close to that of the known $Kr_2(^{1,3}\Sigma_u^+ - X\,^1\Sigma_g^+)$ excimer band (142–152 nm), which correlates with $Kr(5s\ ^3P_{1,2}) + Kr$ [18–22]. Since the intense $Kr(5s\ ^3P_1 \rightarrow 4p^6\ ^1S_0)$ line is actually observed at 123.6 nm, it is highly likely that continuum T is ascribed to the $Kr_2(^{1,3}\Sigma_u^+ - X\,^1\Sigma_g^+)$ excimer. In order to confirm this assignment, emission spectra resulting from the Ar afterglow reactions of Kr were measured, where emission spectra of $HeKr_n^+$ could not be formed. In addition to an intense $Kr(5s\ ^3P_1 \rightarrow 4p^6\ ^1S_0)$ line, two continua appear in the 120–140 and 140–160 nm region, as shown in Fig. 6. The former continuum degraded to red from the Kr^* line is ascribed to the $Kr_2(^{1,3}\Sigma_u^+ - X\,^1\Sigma_g^+)$ transitions from high vibrational levels near the dissociation limit, while the latter continuum with a Gaussian envelope is assigned to those from low vibrational levels to highly repulsive region of the $Kr_2(X\,^1\Sigma_g^+)$ state according to a number of previous spectroscopic data on Kr_2^* excimers [18–22]. The observed wavelength and the spectral features of the third band in Fig. 5 agree well with those in Fig. 6. Therefore, the third continuum was attributed to the $Kr_2(^{1,3}\Sigma_u^+ - X\,^1\Sigma_g^+)$ excimer from low vibrational levels.

In the He^+/Kr system, a discrete peak is found in the 133–137 nm region over a broad continuum in the 115–137 nm region, as shown in Fig. 5d by an arrow. Since this peak is absent in Fig. 6 and it disappears by trapping He^+ in the He flow, He^+ must participate in the formation of this peak. It becomes less prominent with increasing the Kr stagnation pressure, indicating that the collisional relaxation does not take part in the formation of this peak. Similar discrete structures have been observed on the continua in the Ne^+/Rg, Ar^+/Rg, and Kr^+/Xe systems [16].

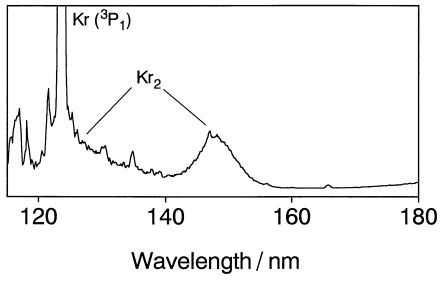

Fig. 6. Emission spectrum obtained from Ar afterglow reactions of Kr at a Kr stagnation pressure of 1.6 atm.

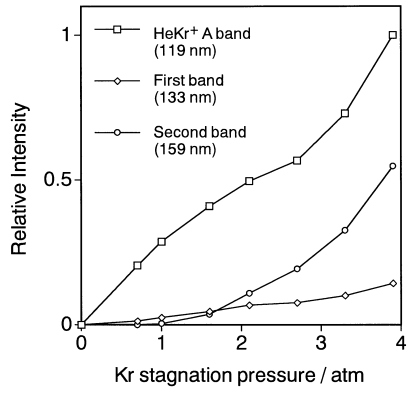

Fig. 7. The dependence of emission intensities of $HeKr^+$ (A band) and continua F and S on the Kr stagnation pressure for the He^+/Kr system.

The dependence of the emission intensities of $HeKr^+$(A band) and continua F and S is shown in Fig. 7. Continuum F appears at a higher stagnation pressure than $HeKr^+$(A band) and increases more rapidly than that with increasing the Kr stagnation pressure. Continuum S appears at a further high Kr stagnation pressure and increases more rapidly than peak F at higher Kr pressures. A comparison of Figs. 3 and 7 implies that the continuous bands appear at lower stagnation pressure below 1.0 atm for the heavier Kr atom and the relative intensity of the second continuum to that of the first one is much larger for the heavier Kr atom. Similar tendencies were found for continua observed from the Ne^+/Ar and Ne^+/Kr systems [16].

The contribution of the collisional relaxation to the observed continua was examined by mixing Ne with Kr as a foreign gas. Fig. 8a–c shows emission spectra obtained by adding various Ne stagnation pressures. The relative intensity of continuum S (159 nm) to that of continuum F (133 nm) increases from 0.09 to 0.2 with increasing the Ne stagnation pressure from 0 to 1.9 atm. This indicates that the

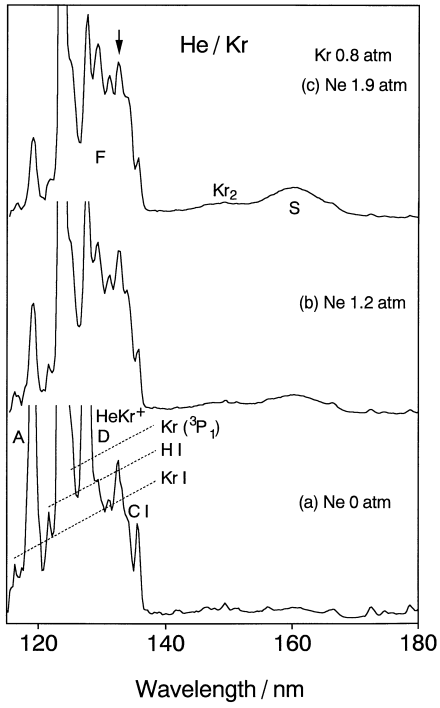

Fig. 8. Emission spectra obtained from He afterglow reactions of Kr by the addition of various stagnation pressures of Ne. The sample Kr gas was kept at a constant stagnation pressure of 1.7 atm. The emission intensities of each spectra are normalized to a discrete peak at 133 nm shown by an arrow.

collisional relaxation is responsible for the formation of the second continuum, as found for the He^+/Ar system. The discrete band with a peak at 133 nm becomes less prominent at high Ne stagnation pressures, indicating that the collisional relaxation does not participate in the formation of this band.

When emission spectra obtained from the He afterglow reaction of Ne were measured at Ne stagnation pressure range of 0–4 atm, the visible $HeNe^+(B^2\Sigma^+–X^2\Sigma^+$ and $B^2\Sigma^+–A_2{}^2\Pi_{1/2})$ band systems were observed at high Ne stagnation pressures. A higher Ne stagnation pressure was required for the formation of $HeNe^+(B)$ than those of Ar and Kr required for the generation of $HeAr^+(B)$ and $HeKr^+(B)$. The emission intensities of the $HeNe^+(B–X, B–A_2)$ bands were much weaker than those of the $HeAr^+(B–X, B–A_2)$ and $HeKr^+(B–X, B–A_2)$ bands. No continua were found from the He afterglow reaction of Ne at Ne stagnation pressures below 4 atm. The reasons for the weakness of the $HeNe^+(B–X, B–A_2)$ bands and the lack of the continua will be discussed in the last part of Section 3.3.

3.2. Possible assignment of the continua and their excitation processes

All the $HeRg^+$ (Rg = Ne, Ar, Kr) bands disappeared when ionic active species, He^+ and He_2^+, were removed from the discharge flow. Combining this result with the fact that the formation of $HeRg^+(B^2\Sigma^+)$ from the He_2^+/Rg reaction is endoergic, the excitation source of $HeRg^+(B^2\Sigma^+)$ is attributed to He^+. Possible excitation processes of $HeRg^+(B^2\Sigma^+)$ at low Rg stagnation pressures are the following two-body radiative association (1) and three-body clustering reaction (2) as reported by Johnsen [8] for the formation of $HeNe^+(B^2\Sigma^+)$ in a flow drift tube.

$$He^+ + Rg \rightarrow HeRg^+(B^2\Sigma^+) + h\nu, \quad (1)$$

$$He^+ + Rg + He \rightarrow HeRg^+(B^2\Sigma^+) + He. \quad (2)$$

In addition, the following clustering reactions are possible at high Rg stagnation pressures:

$$He^+ + 2Rg \rightarrow HeRg^+(B^2\Sigma^+) + Rg, \quad (3)$$

$$He^+ + Rg_n \rightarrow HeRg^+(B^2\Sigma^+) + Rg_{n-1}. \quad (4)$$

In order to examine the relative importance of processes (1) and (2) at low Rg pressures, the dependence of the emission intensity of $HeRg^+(B^2\Sigma^+–X^2\Sigma^+)$ on the He pressure was compared with that of $N_2^+(C^2\Sigma_u^+–X^2\Sigma_g^+)$ resulting from the two-body charge-transfer reaction [23]:

$$He^+ + N_2 \rightarrow N_2^+\left(C^2\Sigma_u^+\right) + He. \quad (5)$$

Measurements were carried out at sufficiently low Rg pressure below 0.05 Torr, where processes (3) and (4) were insignificant. The dependence of $HeRg^+(B^2\Sigma^+–X^2\Sigma^+)$ on the He pressure was similar to that of $N_2^+(C^2\Sigma_u^+–X^2\Sigma_g^+)$ below ~ 0.75 Torr, while a significant enhancement of the emission intensity was found for $HeRg^+(B^2\Sigma^+–X^2\Sigma^+)$ above that. This result indicated that process (1) is dominant at low He pressures below ~ 0.75 Torr, while process (2) is significant above that at low Rg pressures. The new continua also disappeared by removing ionic active species in the discharge flow,

indicating that He^+ and/or He_2^+ are also responsible for the formation of the continua. The continua were observed at low He buffer gas pressures below 1.0 Torr, where the contribution of $[He_2^+]$ was insignificant. It was therefore concluded that the excitation source of the continua is atomic He^+ ion with a high recombination energy of 24.59 eV.

A discrete peak was found in the $HeKr_2^+(B\,1/2–X\,1/2)$ band. Similar discrete peaks due to bound–bound transitions near the dissociation limits appear near the heterodimer bands on both the first and second components of $NeRg_2^+$, $ArRg_2^+$, and $KrXe_2^+$ bands [16]. By analogy with our previous results, the discrete band observed here was attributed to bound–bound transitions from high vibrational states of $B\,1/2$ near the dissociation limits to long-range attractive part of $X\,1/2$.

In this study, new continua were observed in the He^+/Rg reaction system. In Table 1 are summarized the observed wavelengths, energy intervals estimated from the width of the continua, and peak positions along with the wavelengths of the related heterodimer bands. For comparison, our previous data for the Ne^+/Rg system are also shown in Table 1. For $NeRg^+$, five transitions of $A(C_2\,1/2–X\,1/2)$, $B(B\,1/2–X\,1/2)$, $C(C_1\,3/2–A_1\,3/2)$, $D(C_2\,1/2–A_2\,1/2)$, and $E(B\,1/2–A_2\,1/2)$ occur, where the $C_2\,1/2$ state correlates with $Ne^+(^2P_{1/2}) + Rg(^1S_0)$, while the $B\,1/2$ and $C_1\,3/2$ states are derived from $Ne^+(^2P_{3/2}) + Rg(^1S_0)$. The following general tendencies are found for the continua.

(a) The continua consist of two components. The first continuum degraded to the red from near the $HeRg^+(B\,^2\Sigma^+–X\,^2\Sigma^+)$ transition, and the second continuum, a roughly Gaussian feature at longer wavelengths. These spectral features reflect a bound-free character of the transitions from high and low vibrational levels, respectively, by analogy with the well known bound-free continuous bands of Rg_2^* excimers [18–22,24–27]. An enhancement of the second continuum relative to the first one with increasing the stagnation pressure of Rg′ or a foreign gas suggests that the collisional relaxation of the upper vibrational levels to lower ones participates in the formation of the second continuum.

(b) The relative intensity of the second continuum to that of the first one increased significantly, when Rg was replaced from Ar to Kr. The onset stagnation pressure becomes low when Ar atom was replaced by Kr atom with a larger polarizability. These results imply that some clustering reactions with Ar or Kr participate in the formation of the continua.

These features are the same as those found for the continua from the Ne^+/Rg, Ar^+/Rg, and Kr^+/Xe

Table 1
Wavelengths, energies[a], and peak positions of $RgRg'^+$ and $RgRg'^+_2$ for Rg = He and Ne

	He^+				Ne^+			
	dimer (Ref. [1])	trimer (this work)			dimer (Ref. [1])	trimer (Ref. [16])		
	peak position (nm)	wavelength (nm)	energy (cm^{-1})	peak position (nm)	peak position (nm)	wavelength (nm)	energy (cm^{-1})	peak position (nm)
Ne	A band:409.8 D band:423.6	not observed						
Ar	A band:142.6	137–153	6100	~ 149	A band:212.9 B band:216.5 C band:217.7	205–280	13100	229
	D band:145.7	153–168	5800	~ 159	D band:220.3 E band:224.2	250–261	1700	255
Kr	A band:119.3	115–137	14000	~ 130	A band:164.5 B band:166.6 C band:167.3	159–184	8500	172
	D band:127.6	148–170	8700	~ 160	D band:180.8 E band:183.3	184–215	7800	201

[a]Energy width of the observed continuum.

systems, which were ascribed to the $B\,1/2$–$X\,1/2$ and/or $C_1\,3/2$–$A_1\,3/2$ transitions and the $B\,1/2$–$A_2\,1/2$ transition of $RgRg'^{+}_2$, respectively [16]. Thus, by analogy with the above systems, the shorter-wavelength component was attributed to the $B\,1/2$–$X\,1/2$ transition of $HeRg^{+}_2$ and the longer-wavelength component was ascribed to the $B\,1/2$–$A_2\,1/2$ transition of $HeRg^{+}_2$. Here, the $HeRg^{+}_2(B\,1/2,\ A_2\,1/2,\ X\,1/2)$ states correlate with the $HeRg^{+}(B\,^2\Sigma^{+},\ A_2\,^2\Pi_{1/2},\ X\,^2\Sigma^{+}) + Rg(^1S_0)$ dissociation limits, respectively. Possible excitation and relaxation mechanism of $He^{+}Rg^{*}_2$ cluster ions in high and low vibrational levels is the following radiative association processes (6)–(8), clustering reactions (9) and (10), and collisional relaxation process (11):

$$He^{+} + 2Rg \rightarrow He^{+}Rg_2(B\,1/2{:}\text{high}\ v') + h\nu, \quad (6)$$

$$He^{+} + Rg_2 \rightarrow He^{+}Rg_2(B\,1/2{:}\text{high}\ v') + h\nu, \quad (7)$$

$$He^{+}Rg(B\,1/2) + Rg \rightarrow He^{+}Rg_2(B\,1/2{:}\text{high}\ v') + h\nu, \quad (8)$$

$$He^{+}Rg(B\,1/2) + 2Rg \rightarrow He^{+}Rg_2(B\,1/2{:}\text{high}\ v') + Rg, \quad (9)$$

$$He^{+} + Rg_n \rightarrow He^{+}Rg_2(B\,1/2{:}\text{high}\ v') + Rg_{n-2}, \quad (10)$$

$$He^{+}Rg_2(B\,1/2{:}\text{high}\ v') + Rg \rightarrow He^{+}Rg_2(B\,1/2{:}\text{low}\ v') + Rg. \quad (11)$$

Here, $He^{+}Rg$ and $He^{+}Rg_2$ mean that the dominant charge of the ion is located in the He atom.

In this work, we found the $HeRg^{+}_2$ emissions from the $B\,1/2$ state, correlating with the $He^{+}(^2S_{1/2})Rg(^1S_0) + Rg(^1S_0)$ dissociation limit. Although only single electronic state, correlating with $He^{+}(^2S_{1/2})Rg(^1S_0) + Rg(^1S_0)$, is possible for $He^{+}Rg_2(B\,1/2)$, there are three upper states for $Rg^{+}Rg'^{*}_2$ (Rg = Ne, Ar, Kr); the $B\,1/2$ and $C_1\,3/2$ states derived from $Rg^{+}(^2P_{3/2})Rg'(^1S_0) + Rg'(^1S_0)$ and the $C_2\,1/2$ state correlating with $Rg^{+}(^2P_{1/2})Rg'(^1S_0) + Rg'(^1S_0)$ [16]. We have examined the relative contribution of the $B\,1/2$ and $C_1\,3/2$ states and the $C_2\,1/2$ state by isolating $Rg^{+}(^2P_{3/2})$ or $Rg^{+}(^2P_{1/2})$ [16]. The dominant emitting $Rg^{+}Rg'^{*}_2$ states were found to be $B\,1/2$ and/or $C_1\,3/2$ states having $Rg^{+}(^2P_{3/2})$ character. Since the $He^{+}Rg_2(B\,1/2)$ states have $\Omega(=J) = 1/2$ character, there is a difference in the Ω value for the correlating $Rg^{+}(^2P_J)$ state between $He^{+}Rg^{*}_2$ and $Rg^{+}Rg'^{*}_2$ (Rg = Ne, Ar, Kr).

3.3. Possible geometries and potential-energy curves of heterotrimer ions

The energy diagram of $HeAr^{+}_2$ is shown in Fig. 9 as an example of $HeRg^{+}_2$ ions. According to recent ab initio calculations of the ground states of $HeAr^{+}_2$ and $HeNe^{+}_2$ by Wasada et al. [28], their stable geometry is symmetrical triangle (C_{2v}), as shown in Fig. 10a. The $X\,1/2$ and $B\,1/2$ states of $HeRg^{+}_2$ were ascribed to $X\,^2B_2$ and $B\,^2A_1$ on the basis of ab initio data for isovalent Ar_2F and Kr_2F excimers [29]. The Rg–He–Rg angle was evaluated to be 37.4° for $He\cdots Ar^{+}_2(X\,^2B_2)$ and 44.3° for $He\cdots Ne^{+}_2(X\,^2B_2)$. Since the equilibrium internuclear distance of Rg–Rg in $He\cdots Rg^{+}_2(X\,^2B_2)$ was found to be nearly the same as that of known Rg^{+}_2 dimer ions in the ground $X\,^2\Sigma^{+}_u$ state, they concluded that the He atom acts as a host atom of Rg^{+}_2. The dissociation energies of Ar^{+}_2(1.26 eV) and Kr^{+}_2(1.13 eV) are much larger than those of Ar_2(12 meV) and Kr_2(17 meV) in the ground states [30]. Therefore, if the geometry of the emitting $He^{+}Rg_2(B\,1/2)$ state is similar to that of $He\cdots Rg^{+}_2(X\,^2B_2)$, as shown in Fig. 10a, significant blue shifts from the related $HeRg^{+}$ bands are expected for the $He^{+}\cdots Rg_2(B\,^2A_1) \rightarrow He\cdots Rg^{+}_2(X\,^2B_2)$ transitions from high vibrational levels near the $He^{+} + Rg_2$ dissociation limit. The onset wavelengths of the $B\,^2A_1$–$X\,^2B_2$ transitions of $HeAr^{+}_2$ and $HeKr^{+}_2$ are predicted to be 164 and 131 nm, respectively, assuming that the $HeRg^{+}_2$(B–X) emissions occur from high vibrational levels near the $He^{+} + Rg_2$ dissociation limits to $HeRg^{+}_2$ levels near the $He + Rg^{+}_2$ dissociation limits. Namely, the onset wavelengths of the $HeRg^{+}_2(B\,^2A_1$–$X\,^2B_2)$ bands will shift to blue by 24 nm for $HeAr^{+}_2$ and 14 nm for $HeKr^{+}_2$ from the corresponding $HeRg^{+}$(B–X) bands. Although slight blue shifts (3–5 nm) from the related $HeRg^{+}$(B–X) bands were found for the onset wavelengths of the $B\,1/2$–$X\,1/2$ transition of $HeAr^{+}_2$ and $HeKr^{+}_2$, such significant blue shifts could not be observed. These facts led us to conclude that the equilibrium geometry of $He^{+}Rg_2(B\,1/2)$ is signifi-

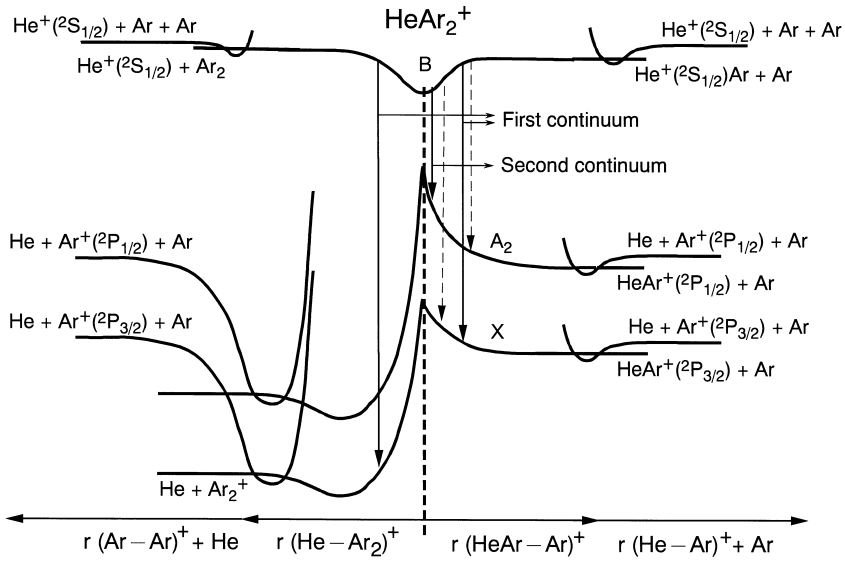

Fig. 9. The potential diagram of the He^+/Ar system.

cantly different from the stable symmetrical triangle geometry of $HeRg_2^+(X\,^2B_2)$. Since the onset wavelengths of the $B\,1/2–X\,1/2$ transitions of $HeRg_2^+$ are located close to those of the related $HeRg^+$ bands, the major chromophore of $HeRg_2^+$ is $HeRg^+$ and the second Rg atom acts as a host atom of He^+Rg in the upper $He^+Rg_2(B\,1/2)$ states. The $B–A_2/B–X$ ratio of $HeKr_2^+$ is larger than that of $HeAr_2^+$. A major reason for this will be the larger $B–A_2/B–X$ ratio of $HeRg^+$ chromophore for Kr (Figs. 2 and 5).

Assuming that $HeRg^+$ is a chromophore and the second Rg behaves as a host atom, most probable equilibrium geometries of the $Rg\cdots He^+Rg\,(B\,1/2)$ state are asymmetrical triangle and linear structures, as shown in Fig. 10b and c, respectively. A He^+Rg_2 molecule in these geometries is in a high vibrational level of antisymmetric stretching mode, and the pho-

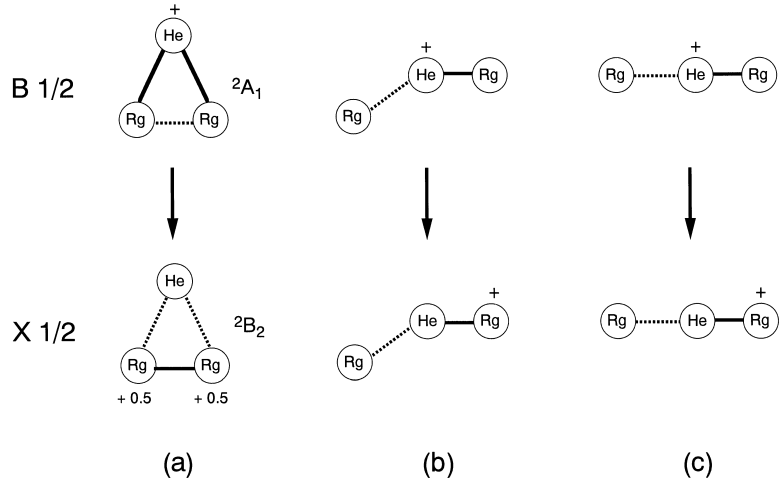

Fig. 10. Possible geometries of the $He^+Rg_2(B\,1/2)$ and $HeRg_2^+(X\,1/2)$ states.

ton is emitted at a turning point, then the He^+Rg molecule would emit as a chromophore. If He^+Rg_2 has linear geometry (c), their maximum transition energies of the first continua will be nearly the same as those of the correlated $HeRg^+$ bands. On the other hand, if He^+Rg_2 has bent geometry (b), blue shifts of the $B\,1/2$–$X\,1/2$ transition due to a bound character of Rg_2^+ will occur for the $HeRg_2^+$ bands. Small blue shifts from the $HeRg^+(B\,^2\Sigma^+$–$X\,^2\Sigma^+)$ bands are actually observed for the $B\,1/2$–$X\,1/2$ transitions of $HeAr_2^+$ and $HeKr_2^+$, as shown in Figs. 2 and 5, respectively. This implies that a minor bound-free transition leading to $He + Rg_2^+$ products (left-hand side route in Fig. 9) as well as a major bound-free transition leading to $HeRg^+ + Rg$ products (right-hand side route in Fig. 9) occurs in these systems. Consequently, the most probable geometry of He^+Rg_2 is asymmetrical triangle structure (b), as predicted for Ne^+Rg_2, Ar^+Rg_2, and Kr^+Rg_2 [16].

Finally, we discuss the origin of the bound-free character of the $He^+Rg_2(B\,1/2) \rightarrow HeRg_2^+(X\,1/2, A_2\,1/2)$ charge-transfer type of transitions. When a charge-transfer type of electronic transition from He^+Rg to $HeRg^+$ in $Rg \cdots He^+Rg(B\,1/2)$ occurs, $Rg \cdots HeRg^+(X\,1/2, A_2\,1/2)$ is formed. The lower $Rg \cdots HeRg^+$ states are much more unstable than the upper $Rg \cdots He^+Rg$ states because of a high $Rg \cdots He$ repulsion at short range. This explains the bound-free character of the heterotrimer bands. The peak shifts of the $HeRg_2^+(B\,1/2$–$X\,1/2)$ transition from the $HeRg^+(B\,^2\Sigma^+$–$X\,^2\Sigma^+)$ transition are 3010 cm^{-1} for $HeAr_2^+$ and 6900 cm^{-1} for $HeKr_2^+$. On the other hand, the peak shifts of the $HeRg_2^+(B\,1/2$–$A_2\,1/2)$ transition from the $HeRg^+(B\,^2\Sigma^+$–$A_2\,^2\Pi_{1/2})$ transition are 5740 cm^{-1} for $HeAr_2^+$ and 15870 cm^{-1} for $HeKr_2^+$. The large peak shifts of the $HeKr_2^+(B\,1/2$–$X\,1/2$, $B\,1/2$–$A_2\,1/2)$ bands from the related heterodimer bands in comparison with the case of the $HeAr_2^+$ bands imply that the $HeKr_2^+(X\,1/2, A_2\,1/2)$ potentials are more repulsive than the $HeAr_2^+(X\,1/2, A_2\,1/2)$ ones. On the other hand, the larger peak shifts of the $HeRg_2^+(B\,1/2$–$A_2\,1/2)$ transitions than those of the $HeRg_2^+(B\,1/2$–$X\,1/2)$ transitions imply that the $A_2\,1/2$ states are more repulsive than the $X\,1/2$ states, as show in Fig. 9. The Franck–Condon overlap integrals for transitions from high vibrational levels of $B\,1/2$ to a higher repulsive $A_2\,1/2$ state will be smaller than those to less repulsive $X\,1/2$ state. This can explain why the $He^+Rg_2(B\,1/2$:high $v')$ state dominantly decays to the $HeRg_2^+(X\,1/2)$ state. The increase in the B–A_2/B–X ratio of $HeRg_2^+$ at high Rg stagnation pressures suggests that the $He^+Rg_2(B\,1/2$:low $v')$ state dominantly decays to the $HeRg_2^+(A_2\,1/2)$ state. This is probably due to the fact that the electronic transition moment of $B\,1/2$:low $v' \rightarrow A_2\,1/2$ is larger than that of $B\,1/2$:low $v' \rightarrow X\,1/2$. In order to confirm above predictions, detailed theoretical calculations of full dimensional potential energy surfaces and Franck–Condon integrals, together with electronic transition dipole moment surfaces for each transition are required.

Although the $HeNe^+(B\,^2\Sigma^+$–$X\,^2\Sigma^+$, $B\,^2\Sigma^+$–$A_2\,^2\Pi_{1/2})$ transitions were observed in the 400–450 nm region from the He afterglow reaction of Ne at high Ne stagnation pressures, their intensities were much weaker than those of the $HeAr^+(B\,^2\Sigma^+$–$X\,^2\Sigma^+$, $B\,^2\Sigma^+$–$A_2\,^2\Pi_{1/2})$ and $HeKr^+(B\,^2\Sigma^+$–$X\,^2\Sigma^+$, $B\,^2\Sigma^+$–$A_2\,^2\Pi_{1/2})$ transitions. The binding energy of $HeNe^+(B{:}D_0' = 292.8\ cm^{-1})$ is much weaker than those of $HeAr^+(1256\ cm^{-1})$, and $HeKr^+(1800\ cm^{-1})$ [2–4]. Thus, the weakness of the $HeNe^+(B$–X, B–$A_2)$ bands was attributed to much weaker binding energy of the B state, so that significant cooling in the reaction zone was required for the formation of the weakly bound $HeNe^+(B\,^2\Sigma^+)$ ion. The lack of $HeNe_2^+$ emission was explained by a lower density of the precursor $HeNe^+(B\,^2\Sigma^+)$ ions and a weaker binding energy of the $Ne \cdots He^+Ne$ bond in the $He^+Ne_2(B\,1/2)$ state.

4. Concluding remarks

Clustering reactions of He^+ with Ne, Ar, or Kr have been studied in a He flowing afterglow at high rare gas stagnation pressures. In addition to known heterodimer emissions, new continua were observed in the longer-wavelength regions of the heterodimer bands except for the He^+/Ne system. They were ascribed to the bound-free $B\,1/2$–$X\,1/2$ and $B\,1/2$–$A_2\,1/2$ transitions of $HeRg_2^+$ heterotrimer ions. In order to confirm this assignment, detailed theoretical calculations of potential surfaces and

transition moments between various electronic states are required including spin–orbit effects. The lack of $HeNe_2^+$ bands was attributed to a low concentration of precursor $HeNe^+(B)$ ion and a weakness of the $Ne \cdots He^+Ne$ binding energy. The continuous bands observed here are new promising species that give excimer lasers in the VUV region. The pumping processes of the upper bound states are expected to be more efficient for Kr than for Ar with a large polarizability because of faster clustering rate coefficients. It is known that the $HeXe^+(B^2\Sigma^+–X^2\Sigma^+$, $B^2\Sigma^+–A_2{}^2\Pi_{1/2})$ transitions occur in the 100–114 nm region [1]. Although $HeXe_2^+$ bands were expected to occur in the longer-wavelength region of these $HeXe^+$ transitions, the optical sensitivity of the VUV monochromator and photomultiplier used in this work was too low to detect emissions below 118 nm. A further high-sensitive experiment below 120 nm was required to study the formation processes of $HeXe^{+*}$ and $HeXe_2^{+*}$.

Acknowledgements

The authors are grateful for Professor S. Yamabe of Nara Educational University and Dr. H. Wasada of Gifu University for providing us their ab initio data prior to publication. This work was partially supported by the Mitsubishi foundation and a Grant-in-Aid for Scientific Research from the Ministry of Education, Science, Sports and Culture (Nos. 06453026 and 09440201).

References

[1] Y. Tanaka, K. Yoshino, D.E. Freeman, J. Chem. Phys. 62 (1975) 4484.
[2] I. Dabrowski, G. Herzberg, J. Mol. Spectrosc. 73 (1978) 183.
[3] I. Dabrowski, G. Herzberg, K. Yoshino, J. Mol. Spectrosc. 89 (1981) 491.
[4] F. Holland, K.P. Huber, A.R. Hoy, R.H. Lipson, J. Mol. Spectrosc. 145 (1991) 164.
[5] K.P. Huber, R.H. Lipson, J. Mol. Spectrosc. 119 (1986) 433.
[6] A. Carrington, C.A. Leach, A.J. Marr, A.M. Shaw, M.R. Viant, J.M. Hutson, M.M. Law, J. Chem. Phys. 102 (1995) 2379.
[7] A. Carrington, C.A. Leach, A.J. Marr, C.H. Pyne, A.M. Shaw, M.R. Viant, Y.D. West, Chem. Phys. Lett. 212 (1993) 473.
[8] R. Johnsen, Phys. Rev. A 28 (1983) 1460.
[9] P. Millet, A.M. Barrie, A. Briot, H. Brunet, H. Dijols, J. Galy, Y. Salamero, J. Phys. B 14 (1981) 459.
[10] C. Laigle, F. Collier, J. Phys. B 16 (1983) 687.
[11] M. Tsuji, M. Tanaka, Y. Nishimura, Chem. Phys. Lett. 256 (1996) 623.
[12] M. Tsuji, M. Tanaka, Y. Nishimura, Chem. Phys. Lett. 262 (1996) 349.
[13] M. Tsuji, M. Tanaka, Y. Nishimura, Chem. Phys. Lett. 266 (1997) 246.
[14] M. Tsuji, M. Tanaka, M. Nakamura, Y. Nishimura, Chem. Lett. (1995) 895.
[15] M. Tsuji, M. Tanaka, M. Nakamura, Y. Nishimura, Chem. Lett. (1996) 367.
[16] M. Tsuji, M. Tanaka, Y. Nishimura, J. Chem. Phys. 107 (1997) 4852.
[17] M. Tsuji, in: J.M. Farrar, W.H. Saunders, Jr. (Eds.), Techniques of Chemistry, vol. 20, ch. 9, Wiley, New York, 1988, p.489.
[18] P.K. Leichner, R. Ericson, Phys. Rev. A 9 (1974) 251.
[19] E.T. Verkhovtseva, E.A. Katrunova, A.E. Ovechkin, Ya.M. Fogel, Chem. Phys. Lett. 50 (1977) 463.
[20] R. Brodmann, G. Zimmerer, J. Phys. B 10 (1977) 3395.
[21] T.D. Bonified, F.H.K. Rambow, G.K. Walters, M.V. McCusker, D.C. Lorents, R.A. Gutcheck, Chem. Phys. Lett. 69 (1980) 290.
[22] E.T. Verkhovtseva, E.A. Bondarenko, Yu.S. Doronin, Chem. Phys. Lett. 140 (1987) 181.
[23] H. Sekiya, M. Tsuji, Y. Nishimura, J. Chem. Phys. 87 (1987) 325.
[24] P.G. Wilkinson, Can. J. Phys. 45 (1967) 1715.
[25] P.K. Leichner, K.F. Palmer, J.D. Cook, M. Thieneman, Phys. Rev. A 13 (1976) 1787.
[26] R. Brodmann, G. Zimmerer, J. Phys. B 10 (1977) 3395.
[27] L. Goubert, E. Desoppere, W. Willem, R. Polák, I. Paidarová, G.D. Billing, J. Phys. Chem. 99 (1995) 15479.
[28] H. Wasada, S. Yamabe, K. Hiraoka, A. Minamitsu, A. Shimizu, M. Nasu, Abstr. Jpn. Annu. Symp. Mol. Struct., Fukuoka 1 (1996) 57.
[29] W.R. Wadt, P.J. Hay, J. Chem. Phys. 68 (1978) 3850.
[30] N.L. Ma, C.Y. Ng, J. Chem. Phys. 99 (1993) 3617.